Supporting Information

Microporous carbon enhanced by structural modifications to suppress polysulfide shuttling and reducing capacity fading in lithium-sulfur batteries

Delvina Japhet Tarimo[1], Francisco J. García-Soriano[2], Alen Vizintin[2], Christian Prehal[3], Elena Tchernychova[2] and Volker Presser[1,4,5,*]

[1] *INM – Leibniz Institute for New Materials, Campus D2 2, 66123, Saarbrücken, Germany*

[2] *National Institute of Chemistry, Hajdrihova 19, Ljubljana, Slovenia*

[3] *University of Salzburg, Department of Chemistry and Physics of Materials, Jakob-Haringer Straße 2a, 5020 Salzburg, Austria*

[4] *Department of Materials Science and Engineering, Saarland University, Campus D2 2, 66123, Saarbrücken, Germany*

[5] *saarene – Saarland Center for Energy Materials and Sustainability, Campus C4 2, 66123 Saarbrücken, Germany*

* Corresponding author: volker.presser@leibniz-inm.de (VP)

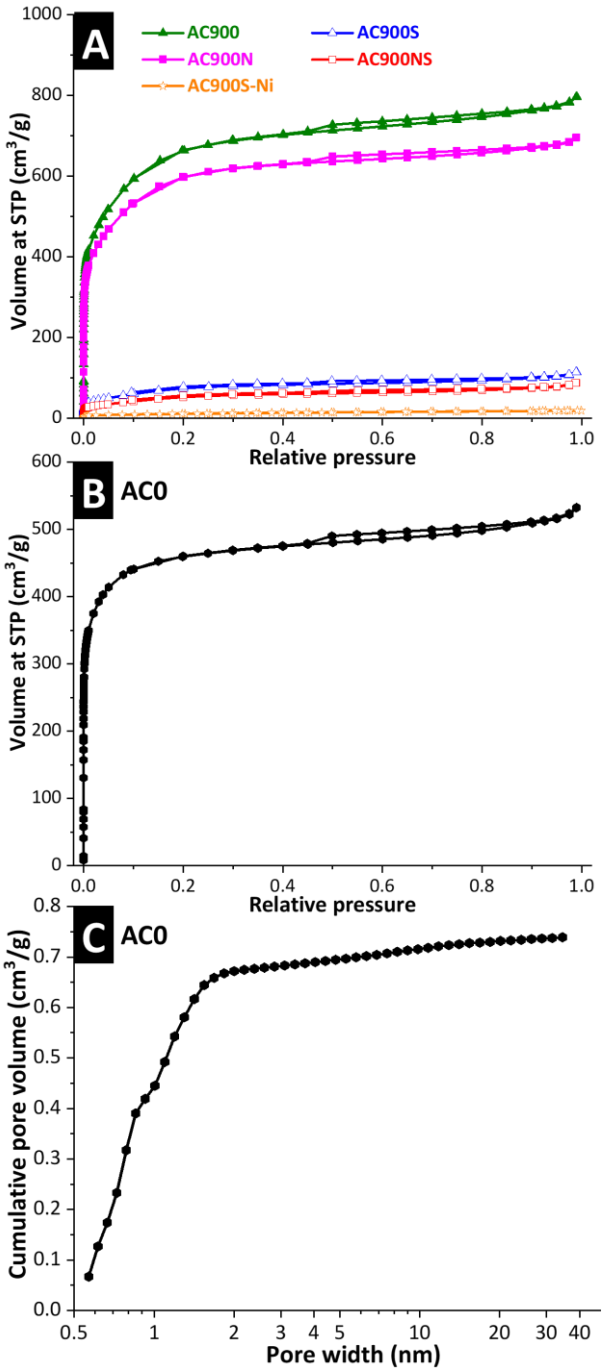

Figure S1: Nitrogen sorption isotherms at -196 °C of AC900, AC900S, AC900N, AC900NS, and AC900S-Ni (A). Nitrogen sorption isotherms at -196 °C of AC (B) and calculated pore size distributions derived from nitrogen gas sorption of AC0 (C).

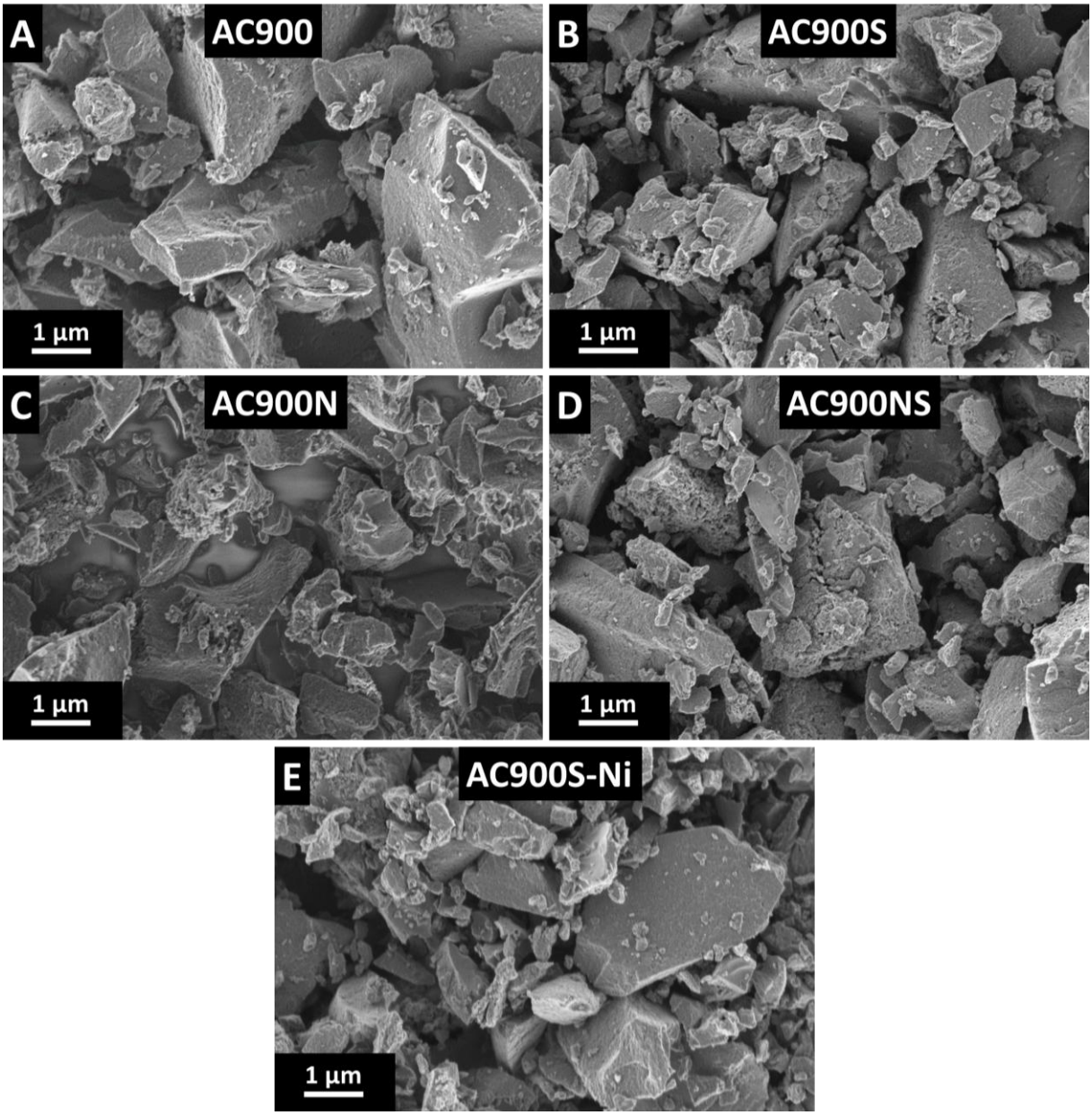

Figure S2: Scanning electron micrographs of the AC900 and AC900S (A-B), AC900N and AC900NS (C-D), and AC900S-Ni (E).

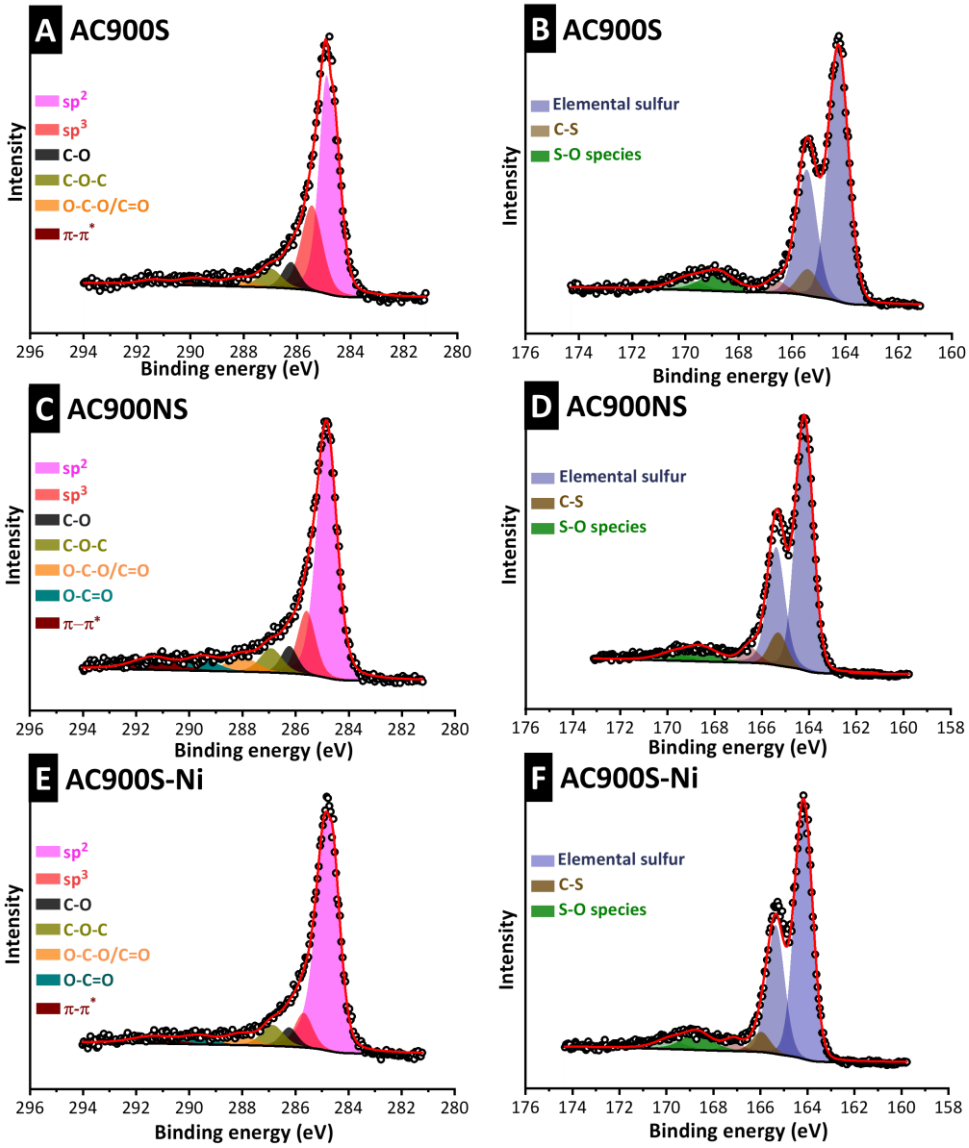

Figure S3: X-ray photoelectron spectra (C 1s) of AC900S, AC900NS and AC900S-Ni (A,C,E), and (S 2p) of AC900S, AC900NS, and AC900S-Ni (B,D,F).

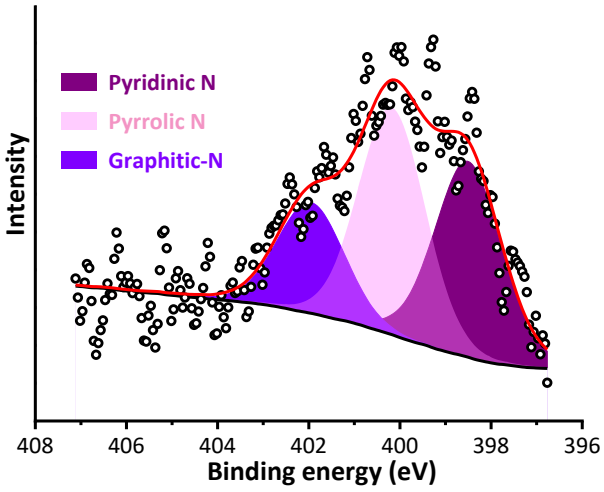

Figure S4: X-ray photoelectron spectrum of N 1*s* of AC900NS.

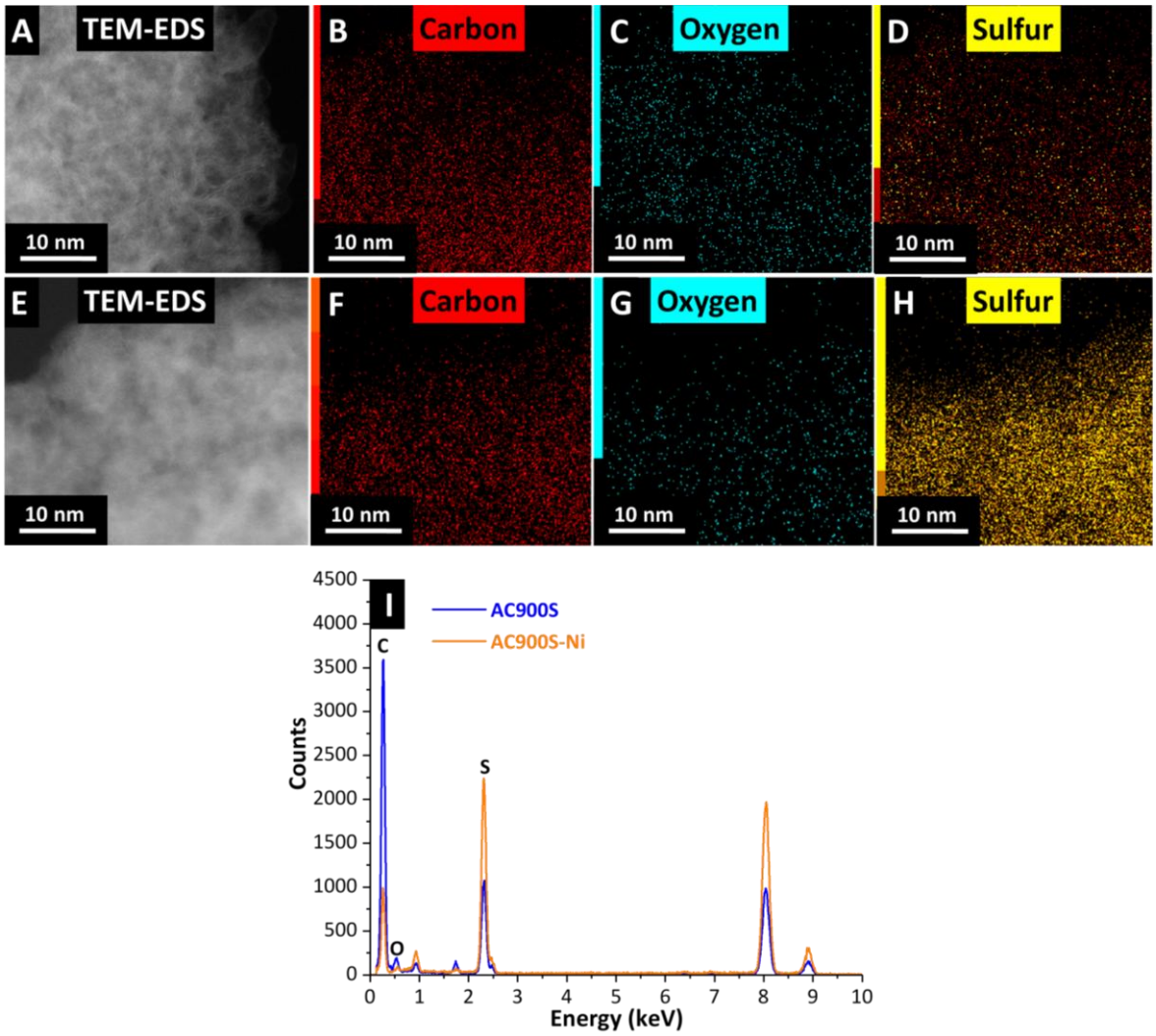

Figure S5: TEM-EDS elemental mapping showing the composition of carbon (B,F), oxygen (C,G), and sulfur (D,H) for AC900S (A-C) and AC900S-Ni (D-F). TEM-EDS spectra of AC900S (G) and AC900S-Ni (H).

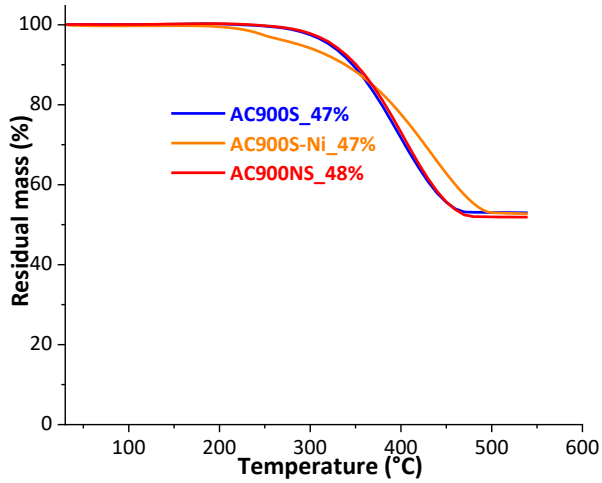

Figure S6: Thermogravimetric analysis to identify the amount of sulfur infiltrated in AC900S, AC900NS, and AC900S-Ni.

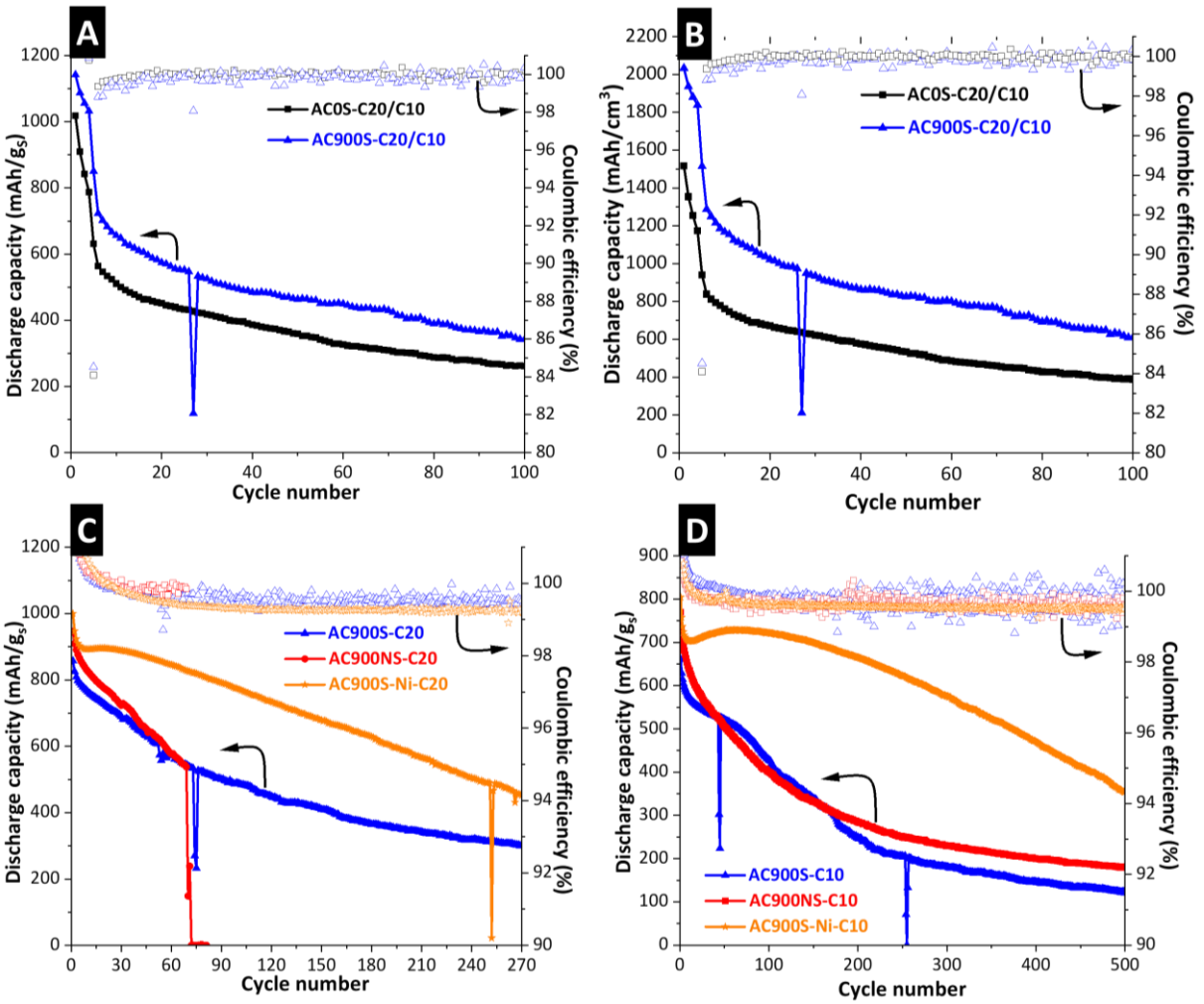

Figure S7: The cycling stability and Coulombic efficiency of AC900S and AC0S performed at 0.5-3.0 V vs. Li/Li$^+$ with C/20 for five formation cycles, followed by 1.0-3.0 V vs. Li/Li$^+$ with C/10 for up to 100 cycles in units of mAh/g$_S$ (A) and mAh/cm^3 (B). The cycling stability and Coulombic efficiency of AC900S, AC900NS, and AC900S-Ni at 1.0-3.0 V vs Li/Li$^+$ with C/20 (C) and C/10 (D). The drop-down points in Figure S7 for AC900S and AC900NS are caused by brief power outages during cycling. These points were removed for better visualization, as can be viewed in the main manuscript in Figure 3C (Figure S7A), Figure 4E (Figure S7C), and Figure 4F (Figure S7D).

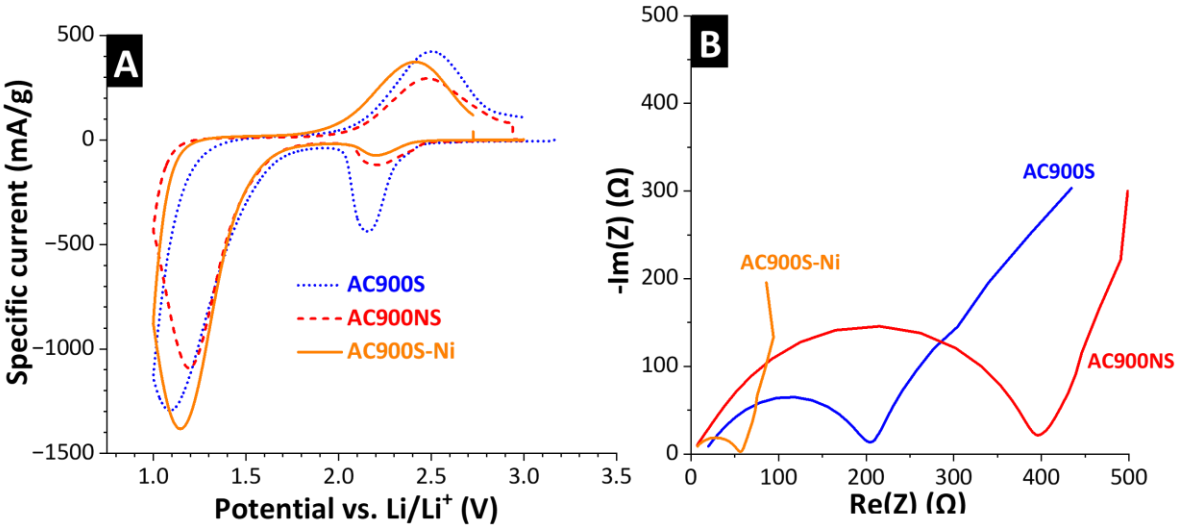

Figure S8: Cyclic voltammograms (A) and Nyquist plots (B) of AC900S, AC900NS, and AC900S-Ni.

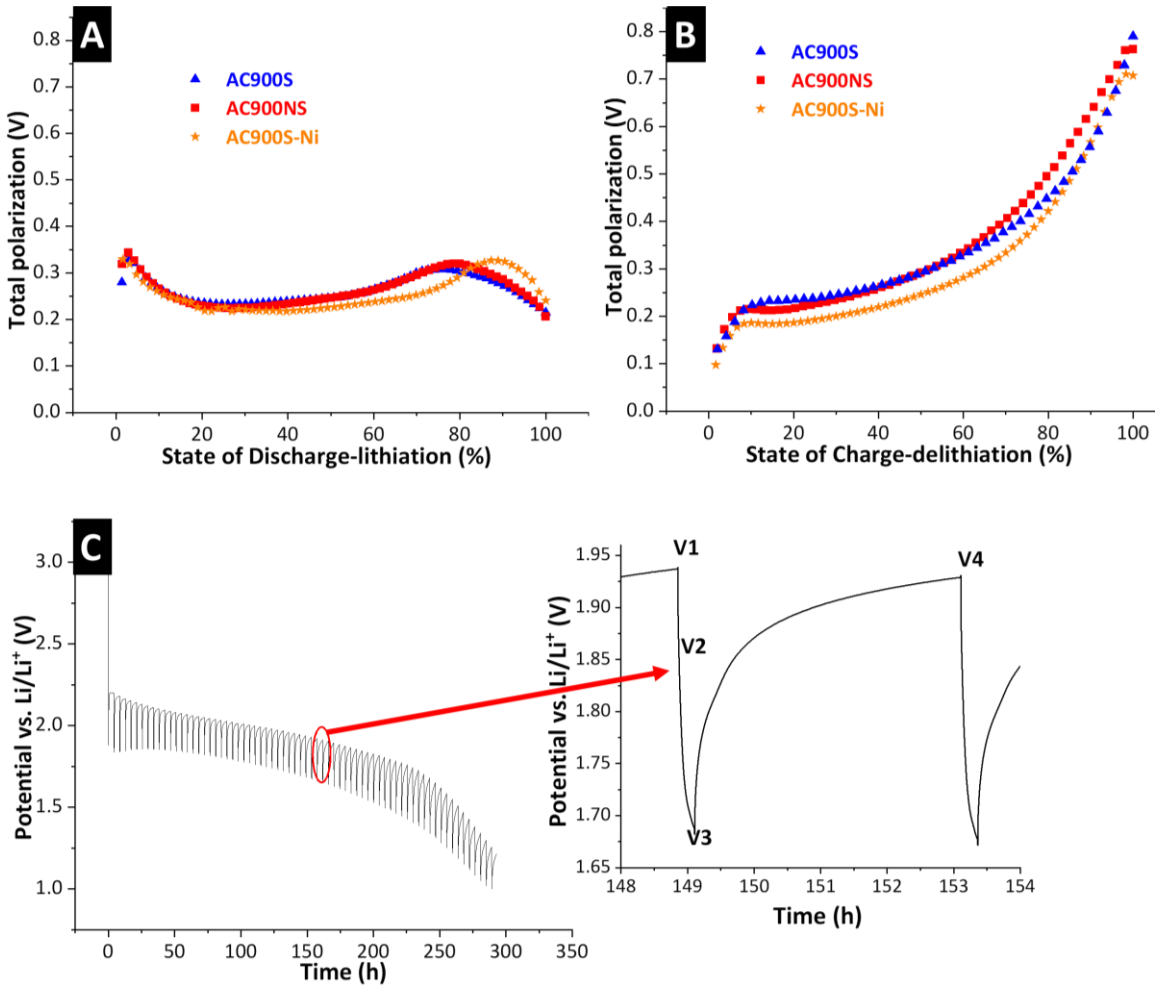

Figure S9: The total polarization as a function of state-of-discharge (SoD) (A) and state-of-charge (SoC) (B). Example of the discharge measured profile with all the potentials involved in the calculation of the GITT analysis (C).

Table S1: The Raman spectra of the carbon D-band and G-band with the fitted position using the Voigt function and full width at half maximum (FWHM).

Sample name	D-band		G-band	
	Position (cm^{-1})	FWHM (cm^{-1})	Position (cm^{-1})	FWHM (cm^{-1})
AC900	1344	126	1596	74
AC900S	1340	115	1599	68
AC900N	1345	116	1601	69
AC900NS	1344	116	1601	69
AC900S-Ni	1339	120	1591	75

Table S2: Specific discharge capacity of AC0S and AC900S performed at 0.5-3.0 V vs. Li/Li^+ with C/20 for cycles 1 to 4, followed by C/10 for cycles 5 and 100 at 1.0-3.0 V vs. Li/Li^+.

Sample name	Discharge specific capacity (mAh/g_S); C/20				Discharge specific capacity (mAh/g_S); C/10	
	Cycle 1	Cycle 2	Cycle 3	Cycle 4	Cycle 5	Cycle 100
AC0S	1018	909	841	788	631	261
AC900S	1142	1088	1056	1032	850	342